Journal of Molecular Graphics and Modelling 29 (2011) 650–656

Contents lists available at ScienceDirect

Journal of Molecular Graphics and Modelling

journal homepage: www.elsevier.com/locate/JMGM

Differences in active-site microarchitecture explain the dissimilar behaviors of PBP5 and 6 in *Escherichia coli*

Chiranjit Chowdhury, Anindya S. Ghosh*

Department of Biotechnology, Indian Institute of Technology, Kharagpur, West Bengal 721302, India

ARTICLE INFO

Article history:
Received 9 August 2010
Received in revised form
10 November 2010
Accepted 15 November 2010
Available online 24 November 2010

Keywords:
Penicillin-binding proteins
DD-carboxypeptidase
Escherichia coli
MODELLER
AutoDock

ABSTRACT

Out of the four DD-carboxypeptidases (DD-CPases) in *Escherichia coli*, only penicillin-binding protein (PBP) 5 performs physiological functions such as maintaining cell shape; its nearest homolog, PBP6, cannot perform such functions. Moreover, unlike PBP6, PBP5 efficiently processes both beta-lactam, and peptide substrates. The crystal structure of PBP5 reveals strong inter-residue hydrogen-bonding interactions around the active site, which favor its catalytic activity. However, the recently solved crystal structure of PBP6 cannot explain the reason for the observed functional discrepancies between the two proteins. Enzymatic analyses indicate that moving the morphology maintenance domain from one protein to another can alter the affinities and activities of PBP5 and 6 toward their substrates. To determine why the activities of these enzymes differ, we used molecular modeling, and docking analyses with substrate-mimetic ligands to estimate how amino-acid alterations in the morphology maintenance domain would affect the structure of PBP and hence its substrate specificity. The results obtained from kinetic analyses were directly correlated to the three-dimensional structures of the PBPs determined through *in silico* analyses, indicating a change in the active-site microarchitectures of PBP5 and 6 as a plausible cause of the difference in their biochemical behaviors.

1. Introduction

The most effective beta-lactam drug targets are the high-molecular-mass penicillin-binding proteins (HMM PBPs) [1]. The HMM PBPs are essential for cell survival and are involved in cell elongation, and septation, whereas the role of low-molecular-mass (LMM) PBPs is less clear, with the exception of PBP5 [2]. Of the seven LMM PBPs in *Escherichia coli*, PBP5 is the best studied with respect to structure, biochemistry, and physiology [3–6]. In contrast, little is known about the function of the nearest homolog of PBP5 in *E. coli*, PBP6. Although PBP5 and 6 share conserved signature motifs at and around their active sites and share substantial sequence identity [7], only the former exhibits a high level of DD-carboxypeptidase (DD-CPase) activity with pentapeptide substrates. PBP6 exhibits DD-CPase activity with smaller, artificial substrates but remains inactive toward larger pentapeptides [8]. Interestingly, PBP6 shows a higher rate of acylation by beta-lactam agents than does PBP5 [8]. To discover the functional domain responsible for DD-CPase activity, chimeric proteins were used that contained a stretch of 20 amino acids around the KTG motif of PBP5 (the morphology maintenance domain, or MMD) that had been swapped [5] with that of PBP6 and vice versa. Replacement of the PBP6 MMD with the PBP5 MMD (creating the chimeric PBP656) restored the DD-CPase activity, but the reverse chimera (PBP565) was inactive [8]. This difference indicated the possibility of structural discrepancies between the two proteins and the possibility of an involvement of the MMD in their structural alterations, although there were no significant changes in gross secondary structure as estimated through circular dichroism (CD) spectroscopic analyses [8]. Therefore, differences in the organization of active-site motifs of these PBPs might explain the variation in their biochemical functions. The crystal structures of soluble PBP5 and 6 are available; however, they do not explain the biochemical and physiological functions seen in PBP6 [6,9]. Moreover, there are no data that explain how the MMD alters the orientation of the active site, which may lead to different biochemical activities. Based on the findings of earlier studies [4,5,8,9], we performed homology modeling to elucidate the differences in microarchitecture seen at the active-site clefts of PBP6, 565 and 656. In addition, docking studies on substrate mimetic ligands and the PBPs focused on the site of the biochemical interactions and the relevant differences between PBP5 and 6.

In this study, we performed *in silico* analyses of PBP5 and 6, as well as their active-site chimeras, to elucidate the microarchitectural differences between these proteins, which may explain the differences in their biochemical behaviors.

* Corresponding author.
E-mail address: anindyain@yahoo.com (A.S. Ghosh).

1093-3263/$ – see front matter © 2010 Elsevier Inc. All rights reserved.
doi:10.1016/j.jmgm.2010.11.009

2. Materials and methods

The primary amino acid sequences of PBP5 and 6 were obtained from the NCBI database (http://www.ncbi.nih.gov/). The amino acid sequences of the soluble (s) PBP6 and chimeric proteins used earlier by Chowdhury et al. [8] were used for model building. For modeling, the restraint-based modeling program MODELLER 9v1 [10] was used. The energy minimization (EM) of the model was performed using Discovery Studio software (Version 1.5; Accelrys Software Inc., San Diego, CA), and Gromacs v 3.3.1 [11] software was used for conducting the molecular dynamics (MD) simulation of all the soluble proteins.

2.1. Three-dimensional model building

Each of the target sequences was converted to the PIR format and used to search for potentially related sequences by using the "profile.build" command of MODELLER. The best template was chosen by comparing the root mean square (RMS) and distance root mean square (DRMS) deviations between the models' atomic positions and respective distances, the differences between their main-chain and side-chain dihedral angles, and the percentage sequence identities. The target sequences were aligned with their corresponding templates, and the three-dimensional (3D) model of each target sequence was calculated using MODELLER. The best model had the lowest value of the MODELLER objective function. Each model was further evaluated by analyzing its DOPE potential using MODELLER.

The homology models of each sPBP that we constructed were improved through EM using the CHARMM version 22 program [12] in the Discovery Studio software suite (Version 1.5; Accelrys Software Inc., San Diego, CA). The models were improved based on the steepest descent energy minimization algorithm with a cutoff distance of 12 Å for non-bonded interactions, a solvent dielectric constant of 1, and a generalized Born solvent dielectric constant of 80 to achieve a reduction in the RMS gradient to under 0.1 kcal/mol Å. The models were further refined by adding explicit water molecules to the MD simulation.

Initially, the box edges of the cubic solid box around the protein lay at least 5 Å away from the protein surface. The box was allowed to fill with simple point charge (SPC) water molecules. Sodium ions (one for sPBP6, four for sPBP656 and three for sPBP565) were used as counterions, bringing the total charge of the system to zero. The 300-ps MD simulations were performed at 300 K using the particle-mesh Ewald method for calculating the electrostatic interactions using the Gromacs program. The conformation at 300 ps was chosen as the 3D structure for further study. PROCHECK [13] and Verify3D [14] (http://nihserver.mbi.ucla.edu/Verify_3D) software were used to evaluate the folding and stereochemistry of all the models.

Because the volume of the active-site groove influences the binding of the substrate and hence the catalysis, the volume of the groove associated with the active-site motifs of the model was measured by surface topography analysis (CASTp) [15].

We analyzed each protein model by the CASTp server (http://cast.engr.uic.edu). The CASTp server identified all the grooves and voids on the protein structures and analytically measured the volume and area of each groove and void. The volume of the groove associated with the signature motifs in each model was selected for further analysis.

2.2. Docking of the substrate mimetic ligand into the sPBPs

A detailed investigation of the mechanism of the DD-CPase reaction with PBP5 was previously described by Shi et al. [16], who docked acylated D-Ala-D-Ala into the PBP5 active site. However, the ligand used in that study was artificial and lacked peptidoglycans. Here, we docked both the artificial (Ac-L-Lys-D-Ala-D-Ala) and pentapeptide (L-Ala-γ-D-Glu-L-Lys-D-Ala-D-Ala) substrates into the active-site clefts of the sPBPs. The docking studies were performed using AutoDock version 4 software (Scripps Research Institute, San Diego, USA) [17,18]. The peptidoglycan mimetic pentapeptide substrate was allowed to dock separately into the entire set of proteins to determine the substrate specificity and the nature of the interactions.

Before docking, the PDB files of the protein molecules were edited by removing the entire water molecules, adding hydrogen atoms (polar and non-polar), adding Gasteiger–Hückel charges and setting the number of torsions (single bonds were considered rotatable and peptide bonds non-rotatable). The grid parameters were set by considering the number of points (60, 60, 60) in the *x*, *y* and *z* coordinates, so that the grid box was positioned and centered around the active-site cleft. The spacing between the grid points was then adjusted to 0.375 Å. This allowed the pentapeptide substrate to dock in an orientation similar to the boronic acid inhibitor (which resembles the portion of the peptide substrate remaining after acylation and loss of the C-terminal D-alanine) which has been shown to bind to the active-site cleft of sPBP5 (PDB ID of sPBP 5 in complex with boronic acid inhibitor is 1Z6F) [19]. The docking parameters were set with a Lamarckian genetic algorithm with the number of energy evaluation set to 250,000. The grid map was generated by AutoGrid and the docking was performed by AutoDock module present in AutoDock 4 suite (http://autodock.scripps.edu/) Finally, the lowest energy docked conformations were combined with the sPBP molecule for further analysis.

3. Results and discussion

The 3D features of the models of sPBP6, 565 and 656 were obtained by homology modeling using MODELLER 9v1. 1Z6F chain A, the crystal structure of PBP5 of *E. coli* in complex with a boronic acid inhibitor [19] at a resolution of 1.60, was chosen as the best template for all the sPBPs. The best template and the target sequence were aligned using Clustal W software [20] to determine their percent identities. Pair-wise sequence alignment indicated that 1Z6F shared 64% identity with sPBP6, 66% with sPBP656, and 98% with sPBP565. With the help of the target sPBP sequences and alignment files, five models were generated by MODELLER, from which the best model was selected by picking the lowest value of the MODELLER objective function and the highest value of negative DOPE potential (a measure of the potential energy of the molecule). All the models had DOPE score profiles similar to that of their template, indicating folds and loops similar to those of their templates. To remove poor steric contacts and achieve a stable conformation, the energy minimizations and dynamics simulations were performed at 300 ps. Upon increasing the temperature, the potential energy initially rose rapidly and then relaxed again to the equilibrium at 300 ps. The average potential energies calculated for sPBP6, 656, and 565 were −1,109,370 kJ/mol, −1,630,870 kJ/mol, and −1,104,430 kJ/mol, respectively.

The final structure (Fig. 1A–C) was further checked using PROCHECK and Verify3D. The PROCHECK analysis indicated that 95.20% of the residues in the sPBP6 model were situated at the most favored region in the Ramachandran plot. The residues with an average 3D-1D score above 0.2 were 90.56%, as determined through the Verify3D. In sPBP656, 93.90% of the residues were placed in the most favored regions in the Ramachandran plot, and 96.44% of the residues had an average 3D-1D score greater than 0.2. In sPBP565, 93.60% of the residues were found in the most favored regions of the Ramachandran plot, and 93.61% of the residues had an average 3D-1D score greater than 0.2. All the protein models were deposited into the PMDB database under the accession num-

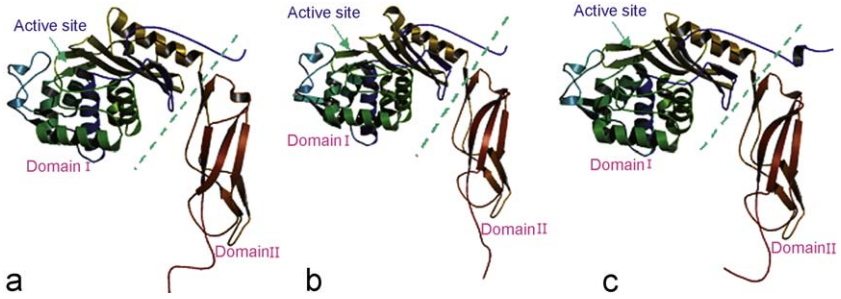

Fig. 1. Homology models of soluble (A) PBP6, (B) PBP656 and (C) PBP565.

bers PMDB0075897, PMDB0075899 and PMDB0075900 for sPBP6, 656 and 565, respectively.

3.1. The active sites of the modeled sPBPs are oriented differently from that of PBP5

Like PBP5, the models are composed of two domains perpendicular to each other. Domain II is mainly β-sheet rich, while, Domain I is composed of both α-helices and β-sheets (Fig. 1A–C). The active site containing the signature motifs (SXXK, SXN, and KTG) lay in the cleft between the five-stranded anti-parallel β-sheet structure and the large α helical cluster of Domain I. To find out whether and how the active-site residues of sPBP6, 565 and 656 are oriented differently from that of sPBP5 (Fig. 2A), the active sites of sPBP6 and the chimeric proteins were superimposed onto the sPBP5 active-site. Their root mean square deviation (RMSD) values indicated a good overall structural alignment with that of sPBP5 (the RMSD value of sPBP5 *versus* sPBP6 is 0.76 Å, that of sPBP5 *versus* sPBP565 is 0.47 Å and that of sPBP5 *versus* sPBP656 the RMSD is 0.54 Å). The overlay model of sPBP6 onto sPBP5 (Fig. 2B) revealed that the orientations of the relevant active-site residues of the SXXK motif were nearly identical (Ser 44 and Lys 47 of sPBP5 *versus* Ser 40 and Lys 43 of sPBP6). However, differences were observed in the orientations of the arginine residues (Arg 198 in sPBP5 and Arg 194 in sPBP6) and the lysine residues (Lys 213 of sPBP5 and Lys 209 of sPBP6, present in KTG motifs) of these proteins. In sPBP5, Lys 213 is located 2.72 Å away from Ser 110 of SXN motif whereas, in sPBP6, the rotation of Lys 209 places it 4.11 Å away from Ser 106 of the SXN motif (Fig. 2B). Compared to Arg 198 in sPBP5, Arg 194 in sPBP6 had undergone a twist along its axis and shifted downward in an anti-clockwise direction (Fig. 2B).

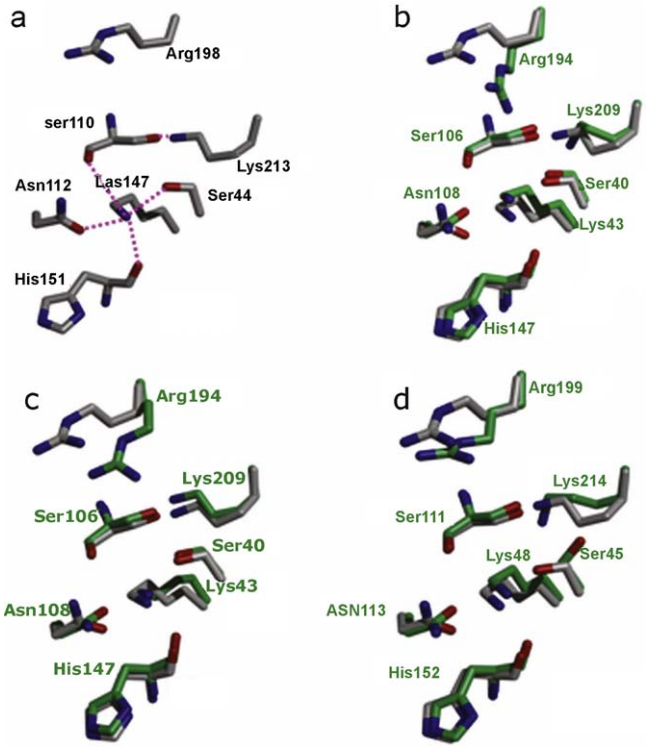

Fig. 2. The active site environments of sPBPs: (A) sPBP5 (1NZO); (B) the stereo overlay of the sPBP5 (1NZO) active-site residues with the active sites of the *in silico* generated models of sPBP6, (C) sPBP656 and (D) sPBP565. The sPBP5 residues are colored in gray and labeled in black; the residues of the other proteins are colored differently and labeled in green. (For interpretation of the references to color in this figure legend, the reader is referred to the web version of the article.)

In sPBP656, the orientations of the residues at the signature motifs caused them to overlap with the corresponding residues of sPBP5, except Arg 194 (Fig. 2C). As in sPBP6, Arg 194 of sPBP656 was shifted downward in an anti-clockwise direction compared to Arg 198 of sPBP5, but unlike sPBP6, it had not undergone any twist along its axis (Fig. 2C).

On the other hand, the signature motifs of sPBP565 were oriented in such a way that they scarcely overlapped with those of sPBP5. In the SXXK motif of sPBP565, the Ser 45 residue was rotated so that it pointed away from Lys 48 instead of pointing toward it, as in sPBP5 (Fig. 2D). However, Ser 45 was imbedded in a highly conserved region on the opposite side of the MMD. Therefore, we speculate that the replacement of the PBP5 MMD with that of PBP6 in sPBP565 had a significant effect on the packing of active-site residues, which may change the orientation of the active-site serine (Ser 45). This altered packing makes the distance between Ser 45 and Lys 48 greater in sPBP565 (4.65 Å) than in sPBP5 (3.15 Å). Although Ser 44 of sPBP5 forms strong hydrogen bonds with Lys 47, the corresponding serine residue (Ser 45) of sPBP565 does not interact favorably with Lys 48 because they are placed too far apart to form hydrogen bonds (which require that the interacting residues lie within 3.6 Å of each other [21]).

In addition, Lys 214 of the KTG motif was rotated so that it was farther from Ser 111 of the SXN motif in sPBP565 (3.99 Å) than in sPBP5 (2.72 Å) (Fig. 2D).

Therefore, because no major differences were observed in the overall structures of all the sPBPs, the differences in orientation of the residues at the active sites of the different PBPs most likely account for the altered biochemical and physiological functions seen in these proteins.

3.2. Active-site groove volumes are changed upon replacement of the MMD

Another factor that affects the binding of the substrate to the active-site cleft is the volume of the cleft. Measuring the groove volume is important; a smaller cleft means a lower chance of the

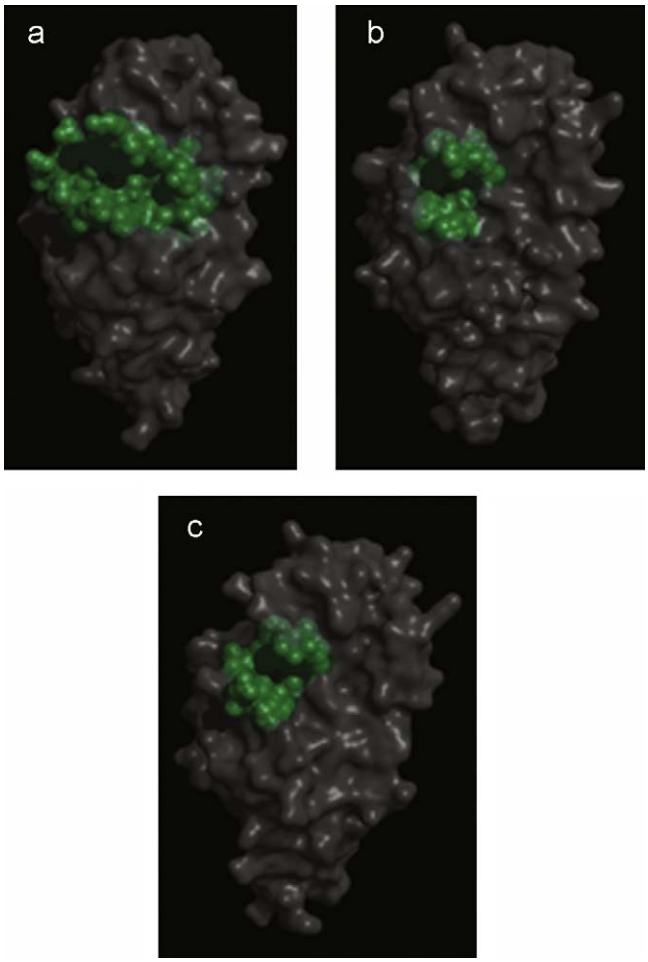

Fig. 3. Comparisons of the active-site cleft volumes of (A) sPBP5, (B) sPBP6, and (C) sPBP656. The residues forming the active-site groove are colored green and space-filled. The orientation of the signature motif of sPBP565 does not allow the formation of a proper active-site cleft.

substrate fitting into the groove [15]. The groove volume surrounding the active-site motif varied between the PBP models. PBP5 had the largest groove volume at its active site (960.8 Å^3) (Fig. 3A), as calculated by the CASTp server [15]. The large groove allows the bulky pentapeptide substrate to bind into the active site of PBP5 during acyl-enzyme complex formation and hence, exerts the DD-CPase function.

When the groove volumes of the PBPs models were compared, the active-site groove of sPBP6 was about one sixth the size (161.5 Å^3) of that of sPBP5 (Fig. 3B). This difference may be caused by the presence of the shortest side chain containing alanine and side-chain-deprived glycine residues at positions 214 and 215, respectively in sPBP6. In contrast, the active-site groove of PBP5 was occupied by amino acids containing longer side chains (Asp 218 and Lys 219) that may help to widen the groove and increase its volume. Grafting the 20 amino acids containing the MMD of PBP5 into PBP6 increases the groove volume to 242.8 Å^3 in sPBP656 (Fig. 3C). The orientation of the active-site motifs in sPBP565 does not allow the formation of a proper active-site cleft for substrate anchoring. The CASTp server was not able to detect the proper substrate binding groove near the signature motifs of sPBP565. The absence of the proper active-site groove may impair substrate binding and the activity of the enzyme, irrespective of the structures of the substrates.

3.3. Discrepancies in the orientation of their active-sites determine the biochemical functions of the sPBPs

In PBP5, favorable interactions between the signature motifs and the surrounding residues help anchor the substrate properly into its active-site cleft and help its hydrolysis [6,22]. A change in the orientation of any of the crucial sPBP5 residues mentioned above would alter its substrate affinity and its hydrolysis. Therefore, it is important to understand how the relative orientation of the active-site residues affects the biochemical behavior of the sPBPs.

There was a strong hydrogen-bonding environment around the signature motif of PBP5 (Fig. 2A) that was favorable for acylation and deacylation. During acylation, Lys 47 of the SXXK tetrad acts as a proton acceptor for a nucleophilic attack by Ser 44, thereby facilitating the formation of an acyl-enzyme intermediate [6,19] (Fig. 4A). In addition, the protonated Lys 213 of the KTG motif forms an electrostatic anchor with the terminal carboxylate group of the peptide stem, thereby aiding in the proper positioning of the substrate during acyl-enzyme complex formation (Fig. 4A) [23]. Additional residues such as Arg 198 of sPBP5 may stabilize the acyl-enzyme intermediate by interacting with the peptide substrate [22], although the mechanisms of this interaction are unclear. During deacylation of the peptide substrate, Ser 110 of the SXN motif and Lys 213 of the KTG motif form a hydrogen-bond bridge with a water molecule. This bond helps position the hydrolytic water molecule toward the carbonyl carbon of the acyl-enzyme complex, thereby facilitating the action of carboxypeptidases (Fig. 4B).

In PBP6, the larger distance between Ser 106 of the SXN motif and Lys 209 of the KTG motif hinders the proper orientation of the hydrolytic water molecule during the hydrolysis of the acyl-enzyme complex. This improper orientation may result in a reduction in DD-CPase activity with the artificial substrate N$^{\alpha}$, N$^{\varepsilon}$-diacetyl-Lys-D-Ala-D-Ala [8]. This situation resembles the one observed in a Lys 213 Arg mutant of PBP5 that lacks DD-CPase activity but retains the ability to bind and hydrolyze penicillin [24]. In this mutant, the distance between Ser 110 and Arg 213 of the SXN motif is too high to form the hydrogen-bond bridge with a water molecule that inhibits DD-carboxypeptidation. However, PBP6 is inert with the pentapeptide substrate L-Ala-γ-D-Glu-L-Lys-D-Ala-D-Ala [8]. The PG substrate may be too large to fit into the narrow active-site cleft of PBP6. A similar situation has been observed in the Thr 217 Ser and Thr 217 Ala mutations [25], where the loss of DD-CPase activity may be correlated with a reduction in the volume of the active-site groove without a significant impact on the binding to penicillin.

The DD-CPase activity of sPBP656 resembled that of sPBP5, whereas sPBP565 exhibited no DD-CPase activity [8] (Fig. 2C). In particular, the distance between Lys 209 and Ser 106 of PBP656 (Fig. 2C) was more like that of PBP5 (Fig. 2A) than that of PBP6 (Fig. 2B), and this feature may explain how the mosaic protein recovers DD-CPase activity that is more similar to that of PBP5. In addition, the higher volume of the active site of sPBP656 (Fig. 3C) compared to that of sPBP6 (Fig. 3B) may contribute to the increased activity by more easily accommodating different substrates. In contrast to sPBP656, the residues of the PBP6 MMD in sPBP565 exhibited altered and unfavorable orientations with respect to each other. The distance between Ser 111 of the SXN motif and Lys 214 of the KTG motif was larger than that in PBP5, as was the distance between Ser 45 and Lys 48 of the SXXK motif (Fig. 2D). These changes may reduce the efficiency of acylation and deacylation reactions, regardless of substrate.

PBP5 possesses a high capacity for deacylation with a beta-lactam substrate [8,26]. The crystal structure of sPBP5 reveals that the orientation of His 151 in the Ω-type loop of PBP5 places it within a favorable H-bond distance to Lys 47 [22,27,28]. This configuration may have helped orient the hydrolytic water molecule during the

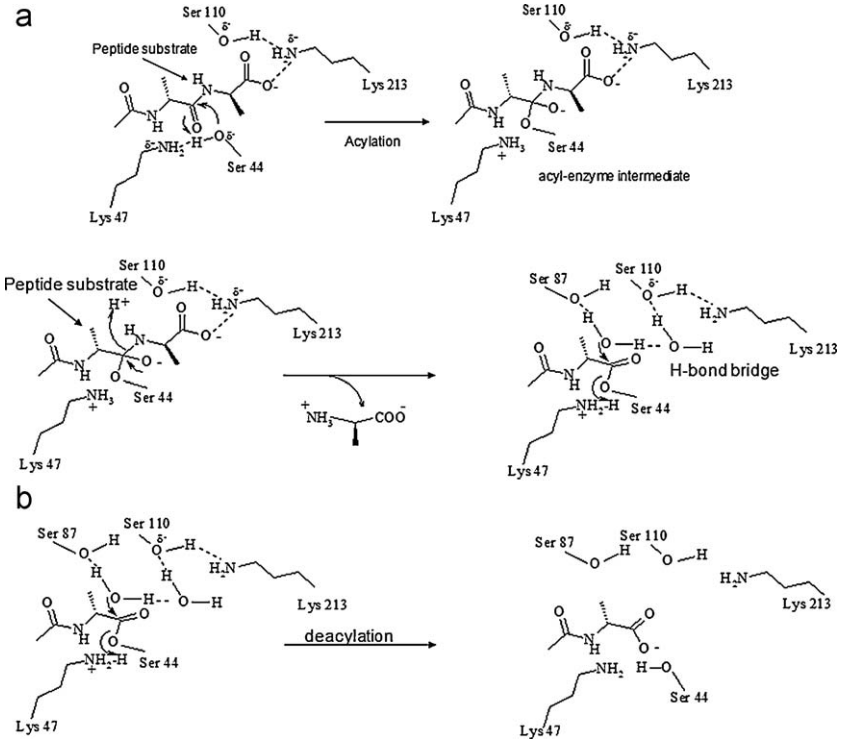

Fig. 4. (A) A schematic representation of the acylation of PBP5 by a peptide substrate. Lys 47 serves as a general base during the nucleophilic attack by Ser 44. Lys 213 forms an electrostatic anchor with the peptide substrate. (B) A schematic representation of the deacylation of the acyl-enzyme complex in PBP5. Ser 110 forms a hydrogen-bond bridge with a water molecule during deacylation.

deacylation of beta-lactams (Fig. 5). The lowering of the deacylation rate of sPBP6 was related to the distance between Lys 43 of the SXXK motif and His 147 in the Ω-type loop, which was larger than that of sPBP5 (in PBP5, the distance was 2.9 Å, whereas in PBP6 the distance was 3.4 Å) (Fig. 5).

3.4. Pentapeptide docking explains the possibility of different substrate specificities among these proteins

DD-CPases remove terminal D-alanine from muramyl pentapeptide and prevent the unwanted crosslink formation which in turn helps in the peptidoglycan remodeling [28]. Therefore, docking of the pentapeptide substrate will facilitate our understanding about the substrate specificities of these PBPs. Although the pentapeptide of *E. coli* consists of L-Ala-γ-D-Glu-m-DAP-D-Ala-D-Ala, the substrate L-Ala-γ-D-Glu-L-Lys-D-Ala-D-Ala was used for docking analyses to correlate the data obtained from enzymatic analysis [8] to the *in silico* predictions. However, we docked L-Ala-γ-D-Glu-m-DAP-D-Ala-D-Ala into all the models and got a result similar to the one obtained by docking with L-Ala-γ-D-Glu-L-Lys-D-Ala-D-Ala (data not shown).

The artificial substrate can dock properly into the active-site clefts of both sPBP6 and sPBP656 in a similar fashion (data not shown), as shown previously for sPBP5 [16]. However, the pentapeptide substrate docks only into sPBP5 and sPBP656 because the smaller active-site groove of sPBP6 cannot accommodate the bulkier pentapeptide into its active site.

The negatively charged carboxy terminus of the peptide substrate interacted with the positively charged residues of the enzyme-ligand complex (Fig. 6A). The orientation of the substrate favored an interaction between the carbonyl carbon connecting the terminal D-alanine residues and the Ser 44 and Lys 47 residues of the SXXK motif. Interactions also occurred between the carboxylate group of the peptide and Lys 213 and Arg 198 of the KTG motif (represented by white dotted lines in Fig. 6A). Such interactions help anchor the peptide substrate inside the cleft and aid in the formation of a tetrahedral intermediate during acylation [19,22,23].

When the MMD of PBP5 is inserted into sPBP6, the groove volume is increased, allowing the pentapeptide to dock in the active site of sPBP656 in a similar manner to that of sPBP5 (Fig. 6B). This docking favors interactions between the active-site residues, Ser 40 and Lys 43 of the SXXK motif, and the carbonyl carbon of the two terminal D-alanines. However, the terminal carboxylate group of

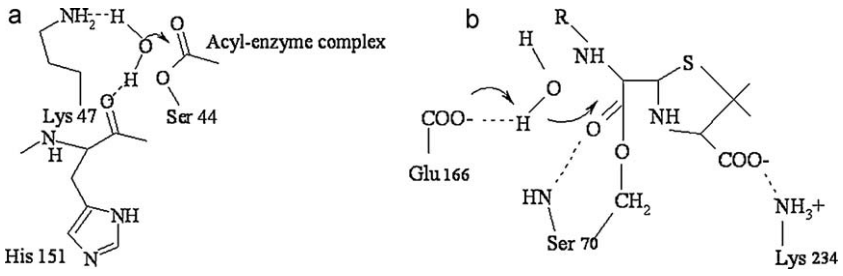

Fig. 5. (A) The involvement of His 151 in the deacylation of the beta-lactam-PBP complex. His 151 of sPBP5 acts similarly to Glu 166 of TEM-1 beta-lactamase (it helps orient the hydrolytic water molecule to the carbonyl carbon of the acyl-enzyme complex [22,27]). (B) Glu 166 of TEM-1 beta-lactamase.

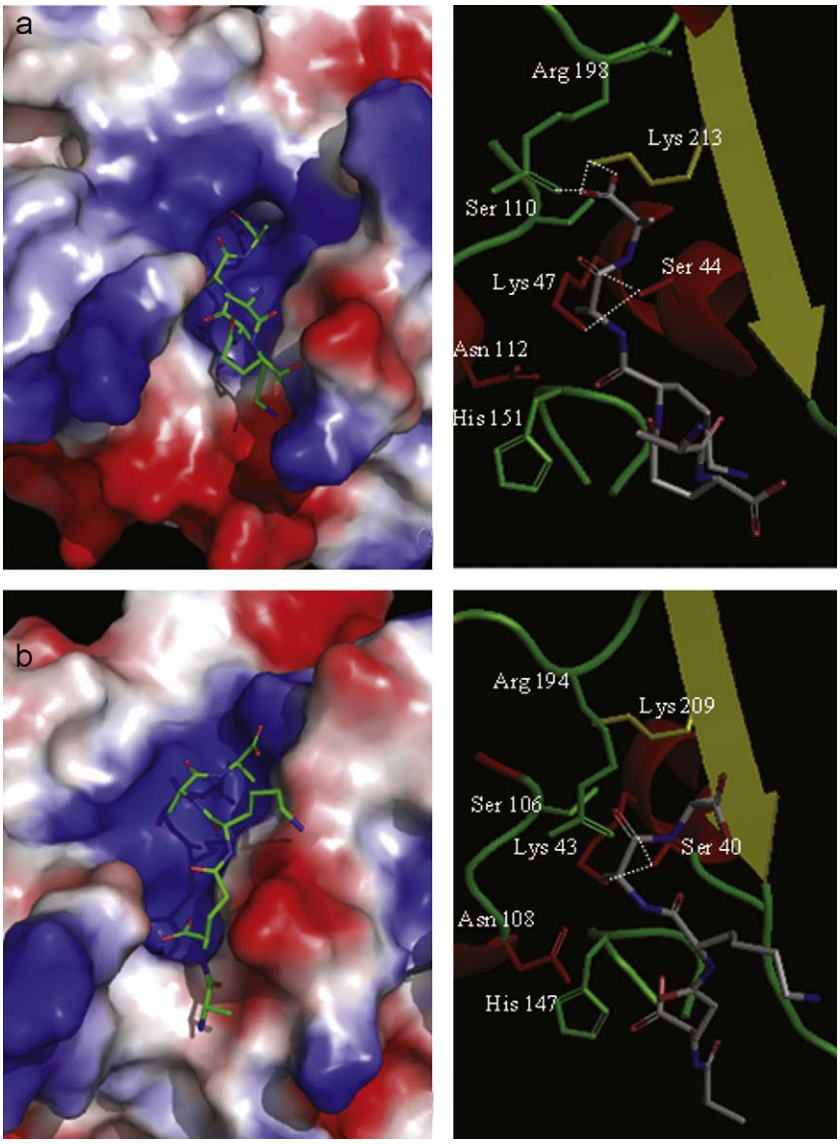

Fig. 6. (A) The docking of the pentapeptide substrate L-Ala-γ-D-Glu-L-Lys-D-Ala-D-Ala into the active-site cleft of sPBP5. Interactions are indicated by white dotted lines. (B) The docking of the pentapeptide substrate L-Ala-γ-D-Glu-L-Lys-D-Ala-D-Ala into the active-site cleft of sPBP656. The pentapeptide substrate is oriented in a fashion similar fashion to that of sPBP5.

the peptide may interact poorly with Lys 209 of the KTG motif and Arg 194, thereby lowering the carboxypeptidase action (Fig. 6B).

3.5. *The PBP6 crystal structure cannot properly explain its biochemical functions*

Unlike the modeled structures, PBP6 is organized as a tetramer in the crystal, with each asymmetric unit organized as a loosely associated dimer of dimers [9]. In the crystal structure, the organization of these two dimers leaves the C-terminal ends of the monomers pointing in opposite directions. It is not clear how the protein is arranged *in vivo*, as the C-terminal parts of all the penicillin-binding proteins are believed to be tethered to the cytoplasmic membranes while the remaining part is free in the periplasm. Therefore, it is unlikely that the C-terminal domain of the inverted monomer will undergo attachment with the outer membrane. Moreover, it is unlikely that the dimer interface (between monomers 3 and 4)-bound pentapeptide substrate can exert DD-CPase activity, as revealed by the crystal structure of PBP6. This observation conflicts with enzymatic analyses of PBP6 that indicate its inactive nature toward the pentapeptide [8] and contradicts the *in vivo* dimeric arrangement of the protein. Furthermore, the complex structure with ampicillin shows a higher distance between Lys 43 and Ser 40 of the SXXK motif (the distance between Lys 43Nζ and Ser 40Oγ is 3.9 Å) [9], which is too distant for hydrogen bond formation; this also raises the question of how an acyl-enzyme complex forms with such antibiotics. Nevertheless, PBP6 exhibits a higher rate of acylation with beta-lactam substrates than does PBP5 [8].

4. Conclusion

In silico studies, including molecular modeling and substrate docking analyses, suggested that the altered affinities and the activities of these proteins toward beta-lactam and pentapeptide substrates were related to discrepancies in the orientation of their active-site clefts, which in turn regulated the biochemical and physiological functions of PBP5 and 6. Therefore, this study provides a rationale for how the asymmetrical organization of the active sites encourages the two proteins to exert different biochemical

and physiological activities despite possessing substantial identities and similar architectures in their overall structures.

Acknowledgement

This work is supported by a grant from the Department of Science and Technology (DST), Govt. of India to ASG.

References

[1] J.M. Ghuysen, Serine beta-lactamases and penicillin-binding proteins, Annu. Rev. Microbiol. 45 (1991) 37–67.
[2] S.A. Denome, P.K. Elf, T.A. Henderson, D.E. Nelson, K.D. Young, *Escherichia coli* mutants lacking all possible combinations of eight penicillin binding proteins: viability, characteristics, and implications for peptidoglycan synthesis, J. Bacteriol. 181 (1999) 3981–3993.
[3] D.E. Nelson, K.D. Young, Penicillin binding protein 5 affects cell diameter, contour, and morphology of *Escherichia coli*, J. Bacteriol. 182 (2000) 1714–1721.
[4] D.E. Nelson, K.D. Young, Contributions of PBP 5 and DD-carboxypeptidase penicillin binding proteins to maintenance of cell shape in *Escherichia coli*, J. Bacteriol. 183 (2001) 3055–3064.
[5] A.S. Ghosh, K.D. Young, Sequences near the active site in chimeric penicillin binding proteins 5 and 6 affect uniform morphology of *Escherichia coli*, J. Bacteriol. 185 (2003) 2178–2186.
[6] R.A. Nicholas, S. Krings, J. Tomberg, G. Nicola, C. Davies, Crystal structure of wild-type penicillin-binding protein 5 from *Escherichia coli*: implications for deacylation of the acyl-enzyme complex, J. Biol. Chem. 278 (2003) 52826–52833.
[7] J.K. Broome-Smith, I. Ioannidis, A. Edelman, B.G. Spratt, Nucleotide sequences of the penicillin-binding protein 5 and 6 genes of *Escherichia coli*, Nucleic Acids Res. 16 (1988) 1617.
[8] C. Chowdhury, T.R. Nayak, K.D. Young, A.S. Ghosh, A weak DD-carboxypeptidase activity explains the inability of PBP 6 to substitute for PBP 5 in maintaining normal cell shape in *E. coli*, FEMS Microbiol. Lett. 303 (2010) 76–83.
[9] Y. Chen, W. Zhang, Q. Shi, D. Hesek, M. Lee, S. Mobashery, B.K. Shoichet, Crystal structures of penicillin-binding protein 6 from *Escherichia coli*, J. Am. Chem. Soc. 131 (2009) 14345–14354.
[10] A. Sali, T.L. Blundell, Comparative protein modelling by satisfaction of spatial restraints, J. Mol. Biol. 234 (1993) 779–815.
[11] D. van der Spoel, E. Lindahl, B. Hess, G. Groenhof, A.E. Mark, H.J. Berendsen, GROMACS: fast, flexible, and free, J. Comput. Chem. 26 (2005) 1701–1718.
[12] B.R. Brooks, R.E. Bruccoleri, B.D. Olafson, D.J. States, S. Swaminathan, M. Karplus, CHARMM: a program for macromolecular energy, minimization, and dynamics calculations, J. Comput. Chem. 4 (1983) 187–217.
[13] R.A. Laskowski, M.W. MacArthur, D.S. Moss, J.M. Thornton, PROCHECK: a programme to check the stereochemical quality of protein structures, J. Appl. Crystallogr. 26 (1993) 283–291.
[14] R. Lüthy, J.U. Bowie, D. Eisenberg, Assessment of protein models with three-dimensional profiles, Nature 356 (1992) 83–85.
[15] J. Dundas, Z. Ouyang, J. Tseng, A. Binkowski, Y. Turpaz, J. Liang, CASTp: computed atlas of surface topography of proteins with structural and topographical mapping of functionally annotated residues, Nucleic Acids Res. 34 (2006) W116–W118.
[16] Q. Shi, S.O. Meroueh, J.F. Fisher, S. Mobashery, Investigation of the mechanism of the cell wall DD-carboxypeptidase reaction of penicillin-binding protein 5 of *Escherichia coli* by quantum mechanics/molecular mechanics calculations, J. Am. Chem. Soc. 130 (2008) 9293–9303.
[17] G.M. Morris, D.S. Goodsell, R.S. Halliday, R. Huey, W.E. Hart, R.K. Belew, A.J. Olson, Automated docking using a Lamarckian genetic algorithm and an empirical binding free energy function, J. Comput. Chem. 19 (1998) 1639–1662.
[18] R. Huey, G.M. Morris, A.J. Olson, D.S. Goodsell, A semiempirical free energy force field with charge-based desolvation, J. Comput. Chem. 28 (2007) 1145–1152.
[19] G. Nicola, S. Peddi, M. Stefanova, R.A. Nicholas, W.G. Gutheil, C. Davies, Crystal structure of *Escherichia coli* penicillin-binding protein 5 bound to a tripeptide boronic acid inhibitor: a role for Ser-110 in deacylation, Biochemistry 44 (2005) 8207–8217.
[20] J.D. Thompson, D.G. Higgins, T.J. Gibson, CLUSTAL W: improving the sensitivity of progressive multiple sequence alignment through sequence weighting, position-specific gap penalties and weight matrix choice, Nucleic Acids Res. 22 (1994) 4673–4680.
[21] W.M Latimer, W.H. Rodebush, Polarity and ionization, J. Am. Chem. Soc. 42 (1920) 1419.
[22] C. Davies, S.W. White, R.A. Nicholas, Crystal structure of a deacylation-defective mutant of penicillin-binding protein 5 at 2.3-Å resolution, J. Biol. Chem. 276 (2001) 616–623.
[23] W. Zhang, Q. Shi, S.O. Meroueh, S.B. Vakulenko, S. Mobashery, Catalytic mechanism of penicillin-binding protein 5 of *Escherichia coli*, Biochemistry 46 (2007) 10113–10121.
[24] K.T. Malhotra, R.A. Nicholas, Substitution of lysine 213 with arginine in penicillin-binding protein 5 of *Escherichia coli* abolishes D-alanine carboxypeptidase activity without affecting penicillin binding, J. Biol. Chem. 267 (1992) 11386–11391.
[25] M.P. van der Linden, L. de Haan, O. Dideberg, W. Keck, Site-directed mutagenesis of proposed active-site residues of penicillin-binding protein 5 from *Escherichia coli*, Biochem. J. 303 (Pt 2) (1994) 357–362.
[26] H. Amanuma, J.L. Strominger, Purification and properties of penicillin-binding proteins 5 and 6 from *Escherichia coli* membranes, J. Biol. Chem. 255 (1980) 11173–11180.
[27] H. Adachi, T. Ohta, H. Matsuzawa, Site-directed mutants, at position 166, of RTEM-1 beta-lactamase that form a stable acyl-enzyme intermediate with penicillin, J. Biol. Chem. 266 (1991) 3186–3191.
[28] A.S. Ghosh, C. Chowdhury, D.E. Nelson, Physiological functions of D-alanine carboxypeptidases in *Escherichia coli*, Trends Microbiol. 16 (2008) 309–317.